Shape Optimisation of an Airship Designed for Atmospheric Pollution Monitoring

Keshav Mohta
Dhirubhai Ambani International School

***Abstract*—Air pollution releases various pollutants which can cause harmful diseases in humans. Accurately monitoring the atmosphere for air pollution is crucial to identify sources, measure concentration of pollutants and analyze the impact of these pollutants on the environment. While there are various solutions including satellites, ground-based monitoring and crowdsourcing data, airships can provide reliable first-party data for a small localised region. This paper details how to find the optimum shape of an elliptical airship that can carry various sensors and electronic components to analyze atmospheric pollution. First, the payload mass was calculated to be 0.608 kg which was then used to determine the volume of the airship as 0.647 m^3. Next, various 2D ellipses with different semi-major and semi-minor axis were tested using computational fluid dynamics (CFD). From these, 5 ellipses with the lowest C_d were selected. Using the volume calculated above, a third dimension was added to these 5 shapes. Then, CFD simulations were conducted on these five 3D shapes to find the optimal ratio of semi-minor to semi-major axis. This was found to be 1:6 and had a C_d of 0.02765.**

***Index Terms*—airship, shape optimization, pollution monitoring, computational fluid dynamics**

I. Introduction

Air pollution is a significant issue today due to various human activities like burning fossil fuels, industrial processes, and agricultural practices. These activities release pollutants such as particulate matter, nitrogen oxides, sulphur dioxide and other volatile organic compounds into the atmosphere. These pollutants can have adverse effects on human health, leading to respiratory problems, cardiovascular diseases, etc. Additionally, air pollution contributes to environmental degradation, including smog formation, acid rain, and ozone depletion. Other ill effects of air pollution are very well documented.

In this context, accurately monitoring the atmosphere for air pollution is crucial to identify sources, measure concentration of pollutants and analyse the impact of these pollutants on the environment. [1] By continuously monitoring air quality, policymakers can make informed decisions to protect public health and the environment, regulate emissions, and mitigate the impacts of air pollution on society.

However, such atmospheric environmental monitoring is challenging due to various reasons. The key difficulty lies in the complexity of air pollution sources and transport processes, which require accurate monitoring to understand and address environmental issues. [2] Air pollution can originate from various sources, including industrial facilities, vehicles, wildfires, and more, making it challenging to pinpoint the exact sources and their contributions to pollution levels. [3] Furthermore, monitoring equipment must be precise and sensitive which requires sophisticated technology and infrastructure. Additionally, weather conditions, such as wind patterns and atmospheric stability, also influence pollutant dispersion and concentration, further complicating monitoring efforts.

There are various solutions that operate from the ground and the air which can help with atmospheric environmental monitoring.

Satellites, through the power of remote sensing, are being widely used for pollution monitoring. They are able to get a macro view of the Earth and identify hot spots of NO_2, SO_2, CO and CH_4 (methane) in semi-urban and urban areas. ESA's TROPOMI and the Korean Space Agency's GEMS are satellites that are currently monitoring the Earth's atmosphere and NASA is also planning on launching pollution monitoring satellites [4]. However, the resolution of these satellites is a few kilometres, which does not allow for more localised pollution detection.

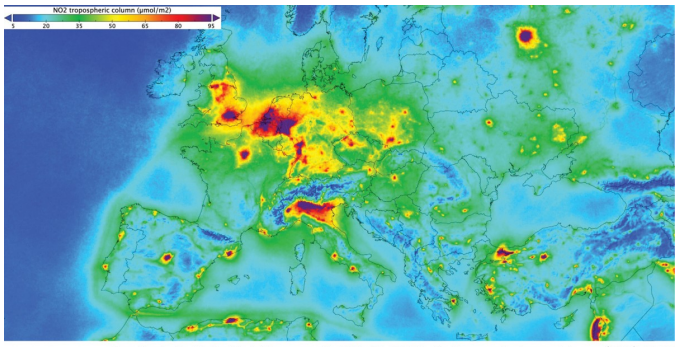

According to the Air Quality in Europe report published in 2018 by the European Environment Agency (EEA), 19 EU Member States recorded nitrogen dioxide concentration above the annual permissible limit. Imagery from Sentinel-5P

Fig. 1. Satellite-based analysis of NO2 concentration over Europe [5]

Ground-based monitoring is done through concrete installations of sensors and other equipment on the ground, usually in urban areas. While they are the simplest solution, ground-based pollution monitoring centres are not mobile, and thus they cannot monitor pollution anywhere else. Furthermore, they are concentrated in urban areas, but as urban areas continue to grow it is very difficult to have pollution monitoring in all parts of the urban area. Mobile and aerial solutions for pollution monitoring might help bring such flexibility.

Fig. 2. Ground based pollution monitoring infrastructure [6]

Crowdsourced data collection is another interesting and effective way of pollution monitoring. Through surveys done on various apps like Google Maps, locals can report pollution levels and possible causes of such pollution. If enough people use these apps and a large amount of data is collected, it is possible to collect reliable data. However, the key challenge with this method is having enough people who can contribute data and are willing to take the effort to fill out pollution surveys.

There were a few issues identified in the current atmospheric monitoring solutions:

1) Satellite monitoring collects data on a very macro level and cannot identify specific pinpoint causes of pollution
2) Ground-based monitoring devices give data about specific locations but aren't mobile and are difficult to use in rural areas
3) Crowdsourced data isn't reliable unless there is enough data collected

To solve these issues, we found that the best possible approach to do such pollution monitoring is using a UAV. The two main UAVs we considered were drones and airships. Drones are far more common and an existing drone can be fitted with the necessary payload and deployed however this would be far more expensive and more importantly, would give a very less flight time, given that it is limited by the drone's battery life. An airship, on the other hand, can fly in the air for a lot longer and thus collect more pollution-related data.

An airship is a dirigible balloon which has the ability to be controlled while flying. Also called as blimps, these devices are a unique, cost-effective, lighter-than-air UAV which can carry payloads into the atmosphere effectively.

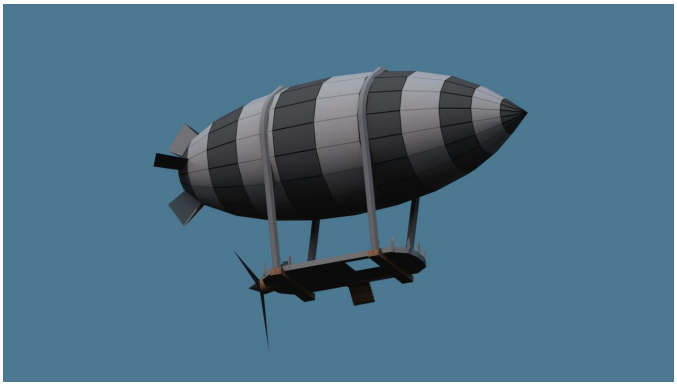

Fig. 3. Illustrated graphic of an airship [7]

The aim of this research was to build such an airship specialised for atmospheric pollution monitoring. The payload needed for such an airship was calculated and using theoretical predictions the necessary volume for the airship was found. Then computational fluid dynamics simulations on Ansys Student helped understand the most optimum shape for the airship.

II. Literature Review

Jiwei Tang et al. [8] aimed to create a methodology to optimise the design of widely used stratospheric airships. The paper describes airships that stay in the air at specific altitudes for long durations, and to keep them running for so long, solar arrays are used to power the airships. The paper optimises the design for the airship by taking into consideration 7 different design variables. Through numerical analysis, they find the optimal output solar array power, envelope shape and solar array layout. A 19.2% reduction in airship volume was achieved. However, the study does not take into account any heat changes in the airship system due to the solar array.

Jafirdaus Jalasabri and Fairuz Izzuddin Romli [9] investigate aerodynamic lift and drag performance of an airship design using CFD, showing how velocity, altitude and design fineness affect aerodynamic characteristics. The paper describes the use of the Star CCM+ analysis tool to analyse the Atlant-100 airship model. It concludes that a low design fineness ratio creates a much larger aerodynamic lift compared to a higher design fineness ratio. However, a higher design fineness ratio produces lower drag, a conflicting conclusion. The paper's main limitation was that the Spalart-Allmaras turbulence model being used was unable to capture the shear forces accurately. It also used only simulations and not experimental data to validate the results.

V. Voloshina et al. [10] compared 4 different turbulence models for airship simulations. The 4 models tested were Realisable two-layer k-ϵ, Standard k-ω, Menter SST k-ϵ and Standard Spallart-Allmaras and were compared for accuracy and resource consumption based on eddy viscosity assumption. A conventional airship model was tested at 3 different angles of attack and the results were compared with wind tunnel experimental data. It was concluded that the Spallart-Allmaras

model is the best model in most cases. The paper does not seem to have any limitations.

Casey Stockbridge et al. [11] presents a generalistic paper evaluating the progress of research in airship development, given the push for environmentally friendly technology. The paper covers new technologies in materials, propulsion (including solar power) and energy storage in airships. It explains how CFD can be used to optimise the shape of an airship and discusses various methodologies for the same. The paper doesn't have any original simulations or experiments, but rather provides an overview of all the progress done in the airship industry.

Keun Woo Shin and Poul Andersen [12] analysed changes in propeller performance upon varying cavity extent over the blade surface. Using DES (Discrete Event Simulation) with a cavitation model, they tested the INSEAN E779A propeller. Propeller performance was measured through thrust and torque. The simulated results were validated by comparing with experimental data. However, experimental data for only two cavitation numbers was found, and the experiment was not validated for all cavitation numbers tested.

Mohammad Irfan Alam et al. [13] worked on optimising the envelope shape of an airship, designed to operate at stratospheric altitudes. The designs were specifically optimised for long endurance missions. The shape was parameterised on four shape coefficients and the airship's length. The residuals between the coordinates of the baseline shape taken from literature and the predicted value using the equation of the airship profile was calculated. By minimising the sum of the residuals squared, optimal shape coefficients were calculated. Then, a composite shape function was formulated by incorporating other parameters like volumetric drag coefficient, area of solar arrays, etc. The optimisation was done through a genetic algorithm and yielded a 1.8% improvement in volumetric drag coefficient and 15% lower circumferential hoop stress. A major limitation was that the algorithm sometimes gave imaginary outputs of the shape function. Additionally, the solar panel area calculation and structural modelling had limitations.

Dheeraj Agarwal et al. [14] developed a framework to optimise the shape of airfoils using open-source CAD and CFD tools. CAD models were directly used for optimization and a workflow between CAD, Mesh and CFD was created. Geometric sensitivities were obtained to calculate gradients with respect to CAD variables and the deformation of the analysis mesh. The framework was tested on a rectangular wing and an airfoil. The aim was to reduce drag while maintaining lift above a certain threshold. A 16.5% reduction in drag was achieved, showing that CAD parameterisation can help in determining optimal shapes while directly modifying CAD geometries. The methodology seems robust and can be applied for different CAD and CFD tools beyond what is tested in the paper.

Wei Qu et al. [15] aimed to optimise and analyse a large-flow, high-pressure fan, specifically the MIX-130 fan, for use in stratospheric airships. The focus was on improving the fan's static pressure rise and efficiency, which was done through a test with five design parameters. These parameters included impeller outlet installation angle, installation angle increment, blade thickness and diffuser tilt angle. After optimization, the fan was processed, and a fan test bench was constructed to validate the numerical analysis method. Performance curves of the fan in both underground and stratospheric conditions were obtained through testing. The static pressure rise increased by 47.5%, while the efficiency saw an 8% increase. Test data confirmed the accuracy of the numerical analysis, with a small average error of 3%. For future scope, a fan parameter optimisation based on an algorithm can be designed to continuously optimise fan performance.

Weicheng Xie et al. [16] conducted biaxial tension tests to predict the effect of temperature on the mechanical properties of airship envelopes, specifically focusing on the UN-5100 material. The study designed and implemented a temperature control device suitable for biaxial tension experiments, allowing for testing at both high and low temperatures. Biaxial tension tests were conducted on UN-5100 membrane specimens across temperatures from -33°C to 80°C. Stress-strain relationships were analysed to determine the elastic modulus and Poisson's ratio of the material under different temperature conditions. It revealed a complex nonlinear stress-strain curve for the UN-5100 membrane in the low-stress direction at each temperature. At low temperatures, both the elastic modulus and Poisson ratio were larger, indicating improved material strength and safety. However, at high temperatures, the material's tolerable strength decreased, posing potential risks during critical daytime conditions. Extending the temperature range for testing could provide a more comprehensive understanding of material behaviour in extreme environmental conditions.

Eiríkur Jónsson [17] worked on creating a computationally efficient methodology for aerodynamic shape optimization using surrogate-based optimisation, instead of direct optimisation, wherein repeated updating and re-optimisation of a computationally cheap surrogate is done. The surrogate is built using a low-fidelity model, on the same equations as a high-fidelity model but with coarser discretisation and relaxed convergence criteria. Using the spaces-mapping methodology this is corrected to a high-fidelity model. This methodology is applicable for low-speed high-lift airfoils and constrained transonic wings. The number of model evaluations are significantly decreased by up to 6 times.

Hatice Cansu Ayaz Ümütlü and Zeki Kiral [18] aimed to optimise the shape of an airfoil, specifically the NACA 4415 profile, to increase its lift coefficient. The methodology involves utilising Bézier curves for parameterization, employing MATLAB for optimization using a genetic algorithm, and conducting flow analysis with XFOIL and ANSYS Fluent. The results indicate a notable enhancement in the lift coefficient of the airfoil. However, the study acknowledges limitations such as being a single-objective optimization and suggests future work to explore multi-objective optimization and experimental validation of the optimised airfoil profile.

R C Morgans et al. [19] utilised numerical optimization techniques for improving objective functions derived from

CFD simulations. Two applications are explored: shape optimization of a low-speed wind tunnel contraction and a simplified test case with a known minimum. The Efficient Global Optimization (EGO) algorithm is employed due to the challenges of complex CFD simulations, which may have long computation times and multiple local minima. EGO efficiently finds the global minimum with minimal function evaluations, demonstrating effectiveness in sampling around the global minimum while avoiding certain local minima. However, the EGO algorithm's performance varied, and improvements are suggested for handling penalty constraints and implementing constraints differently. EGO is effective only for relatively simple problems. A robust stopping criteria could be implemented and expensive optimizations that do not require exact optima could be accommodated to improve.

Sasan Amani et al. [20] utilised a Multi-Objective Optimization (MOO) approach for the design of autonomous airships, considering factors such as aerodynamic drag, static stability, performance, and production cost. Standard airship configurations are divided into three components: the main body (hull), stabilisers, and gondola, with component sizing and positioning crucial for overall stability and performance. MOO analysis aims to achieve optimal interaction among these components, leading to volumetrically optimal designs with desirable characteristics. The paper acknowledges potential inclusion of additional criteria such as aerodynamic lift and airship material, along with the importance of implementing active controls for station keeping and trajectory management.

Current research on airship design optimization faces significant limitations, particularly in the accuracy and efficiency of Computational Fluid Dynamics (CFD) simulations. Many studies rely heavily on CFD for aerodynamic analysis and optimization, but these simulations often lack experimental validation, which questions their reliability. Simplified turbulence models used in CFD, such as Spalart-Allmaras, fail to capture complex shear forces accurately, reducing the precision of aerodynamic predictions. Additionally, computational time remains a critical issue; high-fidelity models demand extensive computational resources and time, making the optimization process cumbersome. Some methodologies attempt to address this by using surrogate models or genetic algorithms to reduce computation time, but they often result in suboptimal or even imaginary outputs. Moreover, experimental data used for validation is sometimes limited, covering only a narrow range of conditions, which further restricts the applicability of the results. The absence of comprehensive heat and material stress analysis under varying environmental conditions also poses a risk, as these factors are crucial for long-duration airship missions.

III. Methodology

The research methodology is depicted in the flowchart below:

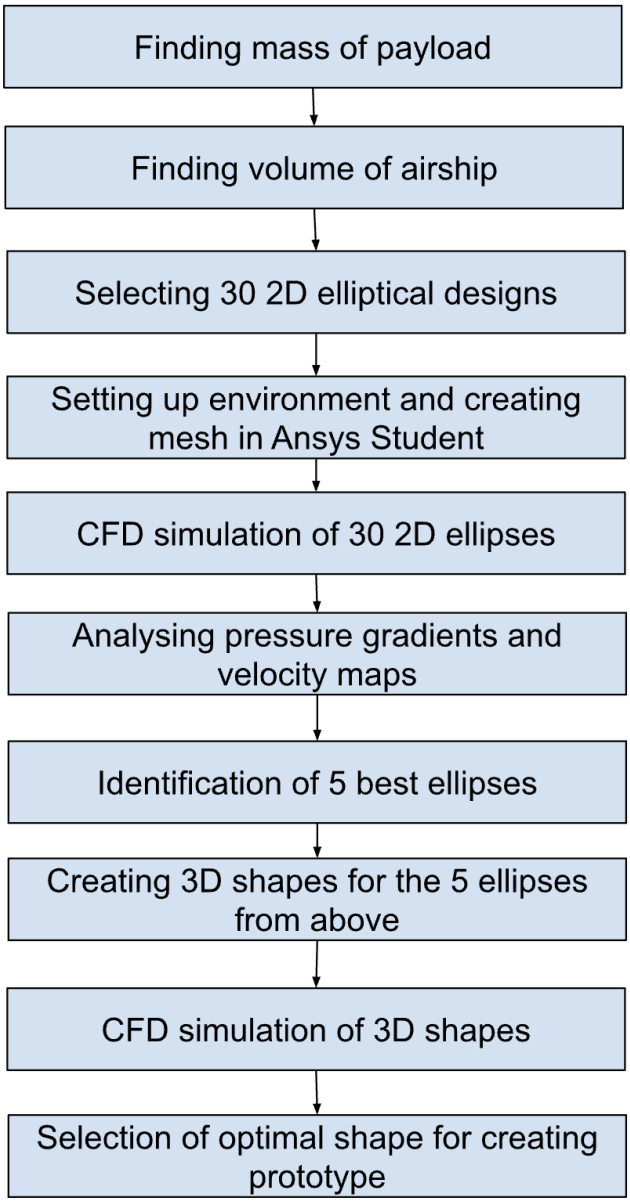

Fig. 4. Flowchart of how the research was carried out

The research started with identifying the requirements of a pollution monitoring airship, including payload mass, altitude and atmospheric conditions. Then, a volume for the airship was calculated. The airship was taken to be an elliptical shape and the dimensions of the ellipse, like the semi-major and semi-minor axis was optimised to reduce drag. The optimisation was done in 2 phases: 2D simulations and then 3D simulations. Doing 2D simulations first ensured that simulation time was not wasted running long 3D simulations on all the design points, but only the ones that had minimal drag.

A. Calculation of payload mass

There are 3 main components to the payload: the electronic equipment, the container that houses the electronic equipment and the fabric of the airship.

The following electronic equipment was considered as part of the airship:

Electronic Equipment	**Purpose**	**Mass**
Arduino Nano	Control for all the other electronic components	7 g [21]
Altimeter	Measure altitude at which the airship is at	140 g [22]
IMU (Inertial Measurement Unit)	Gyroscopes, accelerometers, etc for movement	9 g [23]
AQI Sensors	Sensor array to measure various air quality parameters	300 g
Wires / Misc.	Any other electronic components	30 g
Total Mass		486 g

TABLE I
ELECTRONIC COMPONENTS NEEDED FOR THE PAYLOAD

The container to hold all the electronic equipment would roughly be a cuboidal box of dimensions 0.15 m $\times$ 0.05 m $\times$ 0.05 m made using 2 mm thick balsa wood.

Surface area of cuboidal box = $2(0.15\times0.05+0.15\times0.05+0.05\times0.05) = 0.035$ m^2
Volume of balsa wood needed = 0.035 m^2 $\times$ 0.002 m = 0.00007 m^3
Density of balsa wood = 160 kg m^{-3} [24]
Mass of balsa wood = 0.0007×160 = 0.112 kg = 112 g

Next, the airship itself will be made out of mylar, a thin polyester-based fabric made from PET. We can roughly estimate the mass of this fabric to be 10 g for the entire airship.

Thus, the final payload mass can be calculated like so:

$$486 \text{ g} + 112 \text{ g} + 10 \text{ g} = 608 \text{ g} = 0.608 \text{ kg}$$

B. Empirical and theoretical calculation of airship volume

Using this payload mass, the volume of the airship was estimated.

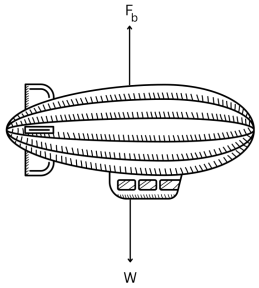

Fig. 5. Free body diagram for an airship

The diagram above shows the forces acting on the airship. The downward force is the weight of the airship i.e. the payload mass and the upward force is the buoyancy force.

For there to be lift, F_b must be greater than W. When they are equal, the volume occupied by displaced air is the minimum volume of the airship.

$$W = mg \tag{1}$$

$$W = 0.608 \times 9.81 = 5.96 \text{ N}$$

$$F_b = \rho V g \tag{2}$$

$$F_b = 1.225 \times V \times 9.81$$

$$W = F_b \Rightarrow 5.96 = 1.225 \times V \times 9.81$$

$$\therefore V = 0.496 \text{ m}^3$$

However, this is the volume assuming that the airship comprises entirely of helium and operates in ideal conditions. Most airships have ballonets, small containers filled with air placed inside the helium-filled airship's envelope. These help moderate large changes in pressure and temperature at high altitudes which could cause helium to excessively expand and break the airship casing. To analyse the effect ballonets could have on our airship, we can try to use the volume calculated above to find a maximum payload mass that can be lifted.

This can be done by first, calculating the lift force due to the airship with ballonets and second, equating that to the payload weight to solve for payload mass.

Equation 3 [25] solves for F_b, the buoyancy force, in terms of ρ_A, the density of air, ρ_{lg}, the density of the lifting gas, I, the inflation fraction and ρ_{ballonet}, the density of air in the ballonets.

$$F_b = (\rho_A - \rho_{lg} \times I - \rho_{\text{ballonet}}(1 - I)) \times V \times g \tag{3}$$

The inflation fraction I refers to the percentage of the volume of helium in the airship compared to the total volume including air-filled ballonets. For commercial airships the inflation fraction is usually 80% so we will use that too. Furthermore, the density of air in Mumbai (where the experiment was conducted), keeping in mind ambient temperature, humidity and air pressure was calculated to be 1.1496 kg m^{-3}. And similarly, the density of helium in Mumbai's conditions was calculated to be 0.21003 kg m^{-3}. The density of air in the ballonets i.e. ρ_{ballonet} is the same as the density of air outside the airship.

Substituting these values into the equation for lift:

$$F_b = (1.1496 - 0.21003 \times 0.8 - 1.1496 \times (1 - 0.8)) \times 0.496 \times 9.81 = 3.657 \text{ N}$$

$$F_b = W \Rightarrow 3.657 = m \times 9.81 \Rightarrow m = 0.373 \text{ kg}$$

This is much lesser than the required payload mass of 0.608 kg.

However, given the airship is designed only to go up til altitudes of 40 m, super-pressure and super-temperature conditions are unlikely to affect the airship and thus the helium won't expand that much.

Thus, the same calculations can be performed for the airship but with no ballonets. If the lift force is calculated without ballonets, the inflation fraction will be 100%.

Calculating the lift force with $I = 100\%$:

$$F_b = (1.1496 - 0.21003 \times 1 - 1.1496 \times (1-1)) \times 0.496 \times 9.81 = 4.572 \text{ N}$$

Consequently, the mass that can be lifted is:

$$F_b = W \Rightarrow 4.572 = m \times 9.81 \Rightarrow m = 0.466 \text{ kg}$$

Thus, there are two observations: firstly, that it is better to use an airship without ballonets and secondly, that even without ballonets under real conditions, a volume of 0.496 m^3 cannot lift the entire 0.608 kg payload mass but can only lift 0.466 kg.

Using the same equation, we can calculate how much volume is needed to lift 0.608 kg:

$$W = F_b = (1.1496 - 0.21003 \times 1 - 1.1496 \times (1-1)) \times V \times 9.81$$

$$\therefore 0.608 \times 9.81 = (1.1496 - 0.21003 \times 1 - 1.1496 \times (1-1)) \times V \times 9.81$$

$$V = 0.647 \text{ m}^3$$

C. CFD Simulations on 2D Shapes

The airship structure was optimised only for ellipses. The dimensions of the ellipse were unknown and had to be optimised.

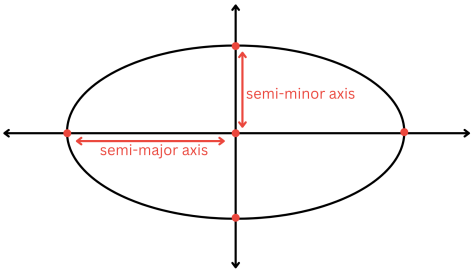

Fig. 6. Ellipse with semi-major and semi-minor axis marked

Figure 6 shows the elliptical schematic for the airship design. The computational fluid dynamics (CFD) simulations will try to optimise the semi-major and semi-minor axis of the airship. These CFD simulations using the finite element method, which divides the 2D ellipse into multiple smaller elements. For each of these smaller elements the governing equations for various parameters are solved and then integrated over the 2D plane to find the coefficient of drag on the entire body.

An effective meshing strategy is crucial for ensuring accurate and efficient results of the simulation. Meshing involves creating these smaller elements of the domain, and it significantly impacts the solution's precision and convergence. The chosen meshing strategy should reflect a balance between computational resources and the desired accuracy of the simulation results. Orthogonality and skewness in the mesh were kept in mind while designing it. Orthogonality refers to the alignment and angle between mesh lines or elements relative to the geometry they represent. High orthogonality indicates that the mesh lines are nearly perpendicular to the boundaries and to each other, which is desirable because it minimises numerical errors and improves the accuracy and stability of the CFD simulation. Poor orthogonality can lead to skewed elements, which can adversely affect the convergence and accuracy of the numerical solution by introducing artificial diffusion and increasing interpolation errors. Thus keeping this in mind, we used a quadrilateral mesh with an inflation of 1.5 around the object.

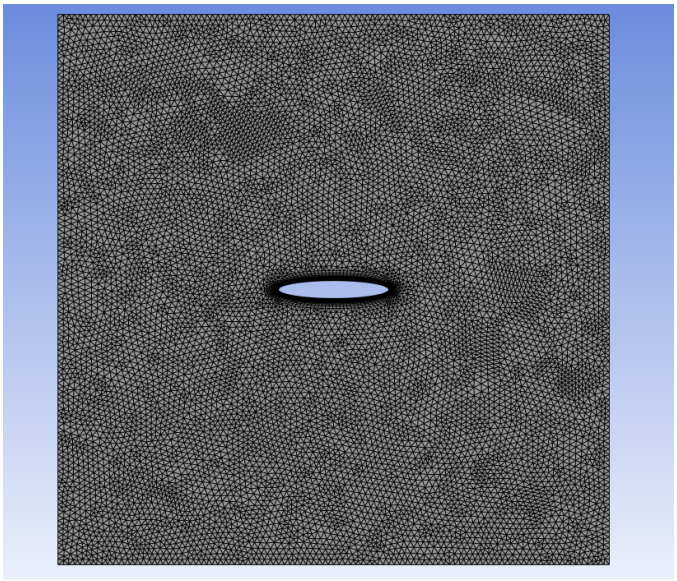

Fig. 7. Mesh for 2D CFD

Both k-ω and k-ϵ models were used for simulation. This is because the k-ϵ model is good for checking external flow and the k-ω model works better on internal flows giving us a holistic view of the shapes we are testing.

30 different ellipses were created with varying semi-major and semi-minor axes and input into Ansys Student, which was then used to calculate coefficients of drag and lift for the airship. Then, we selected the 5 design points with the smallest C_d values.

D. CFD Simulations on 3D shapes

These five 2D shapes were now converted into 3D shapes. Keeping the volume constant at 0.647 m^3, Solidworks was used to create these ellipsoidal shapes.

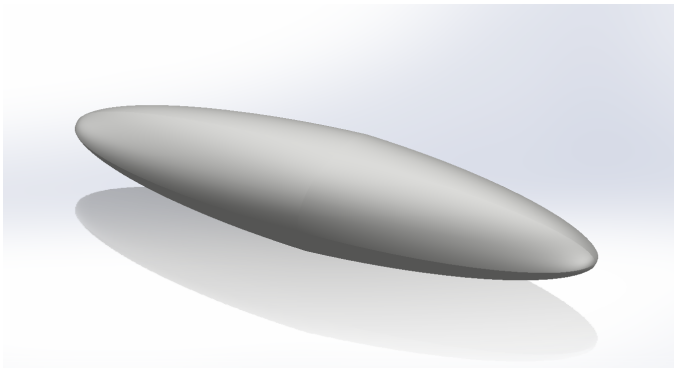

Fig. 8. CAD for one of the ellipsoids

3D CFD simulations were performed on each of the 5 shapes. The shape with least coefficients of drag and highest lift were selected as the most optimum shape of the airship.

IV. Results

Figure 9 below shows the correlation between the semi-minor axis, representative of the vertical height, and the C_d values obtained from the simulation for both $k-\epsilon$ and $k-\omega$ models.

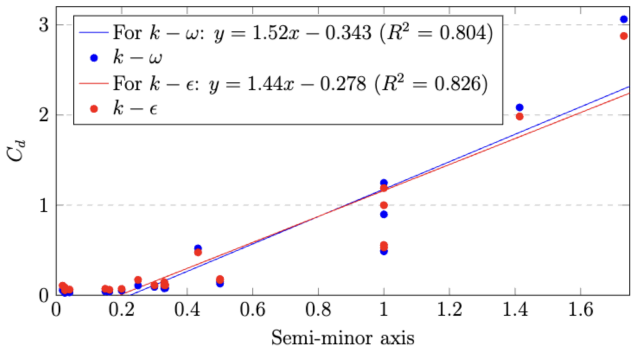

Fig. 9. Semi-minor axis length vs C_d

It shows a moderately positive correlation between both with R^2 values greater than 0.8. This is as expected, as a larger vertical height would cause more interruption to the air flow and smaller vertical heights would allow air to flow easily.

Figure 10 depicts the correlation between the semi-major axis, representative of the horizontal width, and the C_d values obtained from both $k-\epsilon$ and $k-\omega$ models.

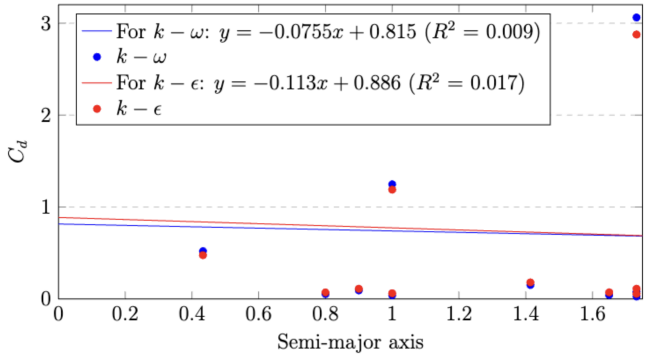

Fig. 10. Semi-major axis length vs C_d

As expected this shows no correlation with very low R^2 values near 0. This means that the horizontal width does not impact the drag at all.

The 5 design points with the smallest C_d values were selected. We calculated the ratio of the semi-minor to the semi-major axis.

Name	Semi-minor axis	Semi-major axis	Ratio
DP 25	0.027	1.732	1:64
DP 16	0.041	2	1:49
DP 27	0.1624	1	1:6
DP 30	0.15	1.65	1:11
DP 19	0.027	3	1:111

TABLE II
BEST 5 ELLIPSES FROM 2D CFD SIMULATIONS

Figure 11 below shows the velocity streamlines plot for DP 27:

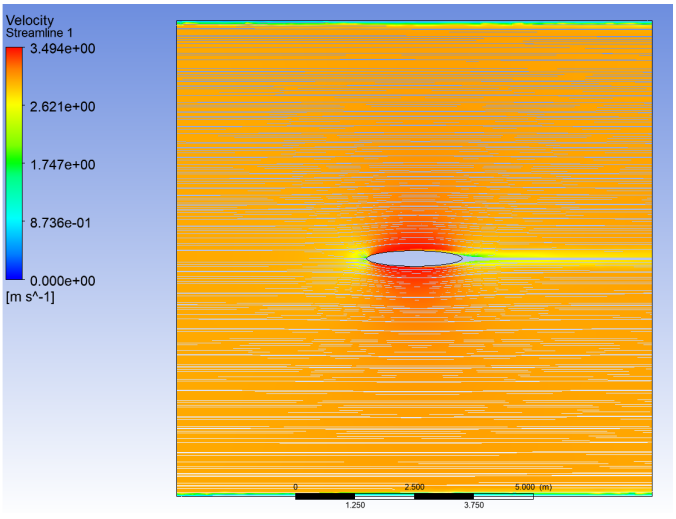

Fig. 11. Velocity streamlines for 2D simulation

We see that the velocity is higher above and below the body indicating that air is bending around the body due to the body

being streamlined and thus having low drag. Furthermore, we also see the wake left behind the airship.

Figure 12 below shows the pressure gradient across the 2D shape:

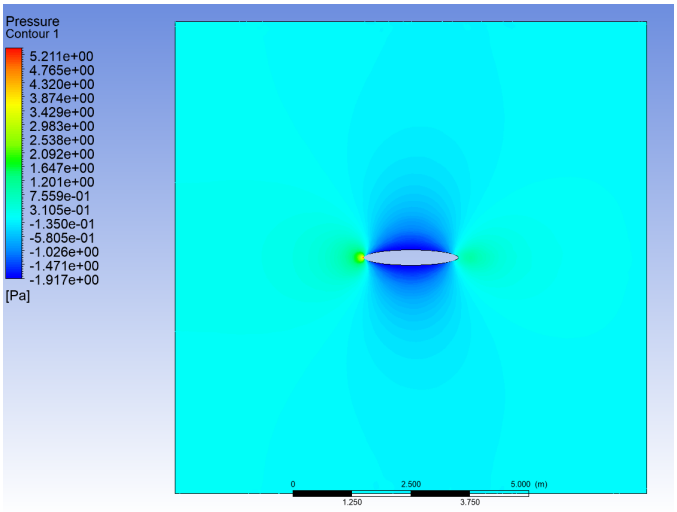

Fig. 12. Pressure for 2D simulation

We see a higher pressure on the left tip, which is where the air hits the shape. This region of higher pressure is very small and concentrated showing how the air gets distributed quickly and drag is minimised.

Figure 13 below shows the velocity streamlines for the 3D simulation.

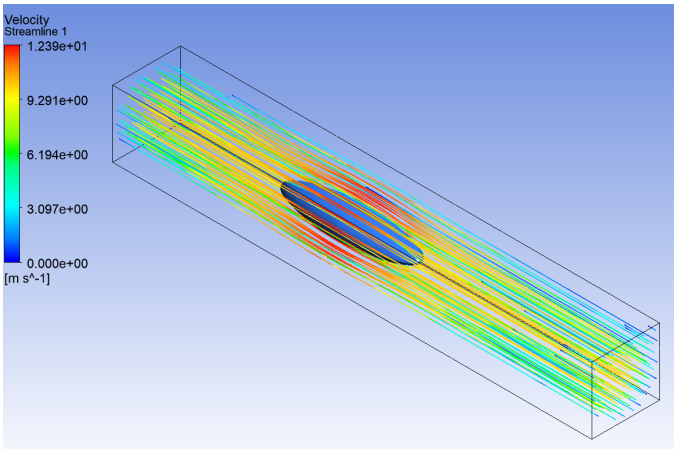

Fig. 13. Velocity streamlines for 3D simulation

We see how the velocity of air is higher near the body, depicting how it is well streamlined and minimises drag.

Figure 14 below depicts pressure around the 3D ellipsoid.

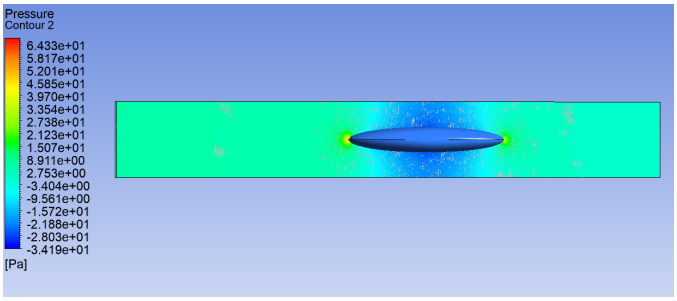

Fig. 14. Pressure for 3D simulation

We see the air pressure surrounding the body. The air inlet is on the left, and there is higher air pressure on the left tip of the body, however this high pressure is very concentrated, showing that drag is minimised.

V. Conclusion

Through this research, a methodology of optimising airship shapes by first testing on 2D shapes and later on 3D shapes has been tested. This was advantageous because it took lesser simulation time while not impacting accuracy of results.

From this research, it has been found that the most optimum dimensions for an elliptical airship are one which has a ratio of semi-minor to semi-major axis of 1:6. This minimises drag and maximises lift. The coefficient of drag C_d obtained from the 3D simulation is 0.02765 which is low and can be used later on in designing control surfaces for the airship.

Furthermore, the CFD simulation helps us see the manufacturing compatibility of the design. The pressure plot for the 3D ellipsoid shows us that there is minimal pressure at the back of the airship and thus control surfaces and propulsion systems can be safely added in the back.

To further this study, the C_d values of the shapes obtained can be validated through experimental testing wherein airship prototypes of different shapes can be built and tested.

References

[1] L. Sun, "Atmospheric environmental monitoring and evaluation based on experimental statistical methods," *E3S Web of Conferences*, vol. 329, 2021.

[2] Y. Sun, T. Yang, H. Gui, X. Li, W. Wang, J. Duan, S. Mao, H. Yin, B. Zhou, J. Lang, H. Zhou, C. Liu, and P. Xie, "Atmospheric environment monitoring technology and equipment in china: A review and outlook," *Journal of Environmental Sciences*, vol. 123, pp. 41–53, 01 2023.

[3] N. P. Service, "Where does air pollution come from? - air (u.s. national park service)," nps.gov, 01 2018. [Online]. Available: https://www.nps.gov/subjects/air/sources.htm

[4] "New satellites tracking air pollution — air quality," airquality.gsfc.nasa.gov. [Online]. Available: https://airquality.gsfc.nasa.gov/new-satellites-tracking-air-pollution

[5] A. Chaturvedi, "How satellites are changing the way we track pollution on the ground," The Wire, 07 2019. [Online]. Available: https://thewire.in/environment/how-satellites-are-changing-the-way-we-track-pollution-on-the-ground

[6] "Ambient air quality monitoring guidelines - perfect pollucon services," Perfect Pollucon Services. [Online]. Available: https://www.ppsthane.com/blog/ambient-air-quality-monitoring-guidelines

[7] "Small airship - blimp 3d model - free3d," free3d.com. [Online]. Available: https://free3d.com/3d-model/small-airship-blimp-1983.html

[8] J. Tang, W. Xie, P. Zhou, H. Yang, T. Zhang, and Q. Wang, "Multidisciplinary optimization and analysis of stratospheric airships powered by solar arrays," *Aerospace*, vol. 10, no. 1, p. 43, Jan 2023.

[9] J. Jalasabri and F. I. Romli, "Computational fluid dynamics (cfd) study on a hybrid airship design," *International Review of Mechanical Engineering (IREME)*, vol. 11, no. 8, p. 573, Aug 2017.

[10] V. Voloshin, Y. Chen, and R. Calay, *A comparison of turbulence models in airship steady-state CFD simulations*, 2012. [Online]. Available: https://arxiv.org/pdf/1210.2970

[11] C. Stockbridge, A. Ceruti, and P. Marzocca, "Airship research and development in the areas of design, structures, dynamics and energy systems," *International Journal of Aeronautical and Space Sciences*, vol. 13, pp. 170–187, 06 2012.

[12] K. W. Shin and P. Andersen, *CFD Analysis of Ship Propeller Thrust Breakdown*, 2019. [Online]. Available: https://backend.orbit.dtu.dk/ws/portalfiles/portal/200381187/SMP19_CavThrust_rev1.pdf

[13] M. Alam, S. Subhani, and R. Pant, *Multidisciplinary Shape Optimization of Stratospheric Airships Multidisciplinary Shape Optimization of Stratospheric Airships*, 2014. [Online]. Available: https://hal.science/hal-01495664/document

[14] D. Agarwal, S. Marques, and T. T. Robinson, "Aerodynamic shape optimisation using parametric cad and discrete adjoint," *Aerospace*, vol. 9, no. 12, p. 743, Nov 2022.

[15] W. Qu, W. Gong, C. Chen, T. Zhang, and Z. He, "Optimization design and experimental verification for the mixed-flow fan of a stratospheric airship," *Aerospace*, vol. 10, no. 2, p. 107, Feb 2023. [Online]. Available: https://www.mdpi.com/2226-4310/10/2/107

[16] W. Xie, X. Wang, J. Tang, Y. Chen, and J. Wu, "Experimental study on the influence of temperature on the mechanical properties of near-space airship envelopes," *Aerospace*, vol. 10, no. 5, p. 413–413, Apr 2023.

[17] E. Jónsson, *AERODYNAMIC OPTIMIZATION BY VARIABLE-RESOLUTION MODELING AND SPACE MAPPING*, 2012. [Online]. Available: https://skemman.is/bitstream/1946/12684/1/Jonsson_2012.pdf

[18] H. C. A. Ümütlü and Z. Kiral, "Airfoil shape optimization using bÉzier curve and genetic algorithm," *Aviation*, vol. 26, no. 1, p. 32–40, Mar 2022.

[19] R. C. Morgans, C. J. Doolan, and D. W. Stephens, *Derivative Free Global Optimisation of CFD Simulations*, Dec 2007. [Online]. Available: https://espace.library.uq.edu.au/data/UQ_120968/Morgans_afmc_16_07.pdf?Expires=1718876747

[20] S. Amani, S. H. Pourtakdoust, and F. Pazooki, "Multi-objective conceptual design optimization of a domestic unmanned airship," *Journal of Theoretical and Applied Mechanics*, vol. 52, pp. 47–60, 01 2014.

[21] Arduino, "Arduino nano," Arduino Official Store. [Online]. Available: https://store.arduino.cc/products/arduino-nano

[22] "200m mini altimeter kit smart sensor," www.airmar.com. [Online]. Available: https://www.airmar.com/Product/200m-Mini-Altimeter-Kit-Smart-Sensor

[23] "Waveshare 10 dof imu sensor," Amazon.in, 2024. [Online]. Available: https://www.amazon.in/DOF-IMU-Sensor-Measurement-Performance/dp/B06WGMYMGL

[24] "Ochroma," Wikipedia, 06 2020. [Online]. Available: https://en.wikipedia.org/wiki/Ochroma

[25] R. S. Pant, "Methodology for determination of baseline specifications of a nonrigid airship," *Journal of Aircraft*, vol. 45, no. 6, p. 2177–2182, Nov 2008. [Online]. Available: https://www.aero.iitb.ac.in/~airships/WEBPAGES/PDFs/ipaper04.pdf